Nuclear Technology

ISSN: 0029-5450 (Print) 1943-7471 (Online) Journal homepage: https://ans.tandfonline.com/loi/unct20

Evaluation of Pulsed Sphere Time-of-Flight and Neutron Attenuation Experimental Benchmarks Using MCNP6's Unstructured Mesh Capabilities

Joel A. Kulesza & Roger L. Martz

To cite this article: Joel A. Kulesza & Roger L. Martz (2016) Evaluation of Pulsed Sphere Time-of-Flight and Neutron Attenuation Experimental Benchmarks Using MCNP6's Unstructured Mesh Capabilities, Nuclear Technology, 195:1, 44-54, DOI: 10.13182/NT15-121

To link to this article: https://doi.org/10.13182/NT15-121

ANS

NUCLEAR TECHNOLOGY · VOLUME 195 · 44–54 · JULY 2016

Evaluation of Pulsed Sphere Time-of-Flight and Neutron Attenuation Experimental Benchmarks Using MCNP6's Unstructured Mesh Capabilities

Joel A. Kulesza[a]* and Roger L. Martz[b]

[a]*University of Michigan, Cooley Laboratory, 2355 Bonisteel Boulevard, Ann Arbor, Michigan 48105*
[b]*Los Alamos National Laboratory, P.O. Box 1663, Los Alamos, New Mexico 87545*

Received September 11, 2015
Accepted for Publication November 16, 2015
http://dx.doi.org/10.13182/NT15-121

Abstract — *This paper extends the verification and validation of MCNP6's unstructured mesh (UM) features for neutron transport capabilities by comparing code and experimental results for two different sets of experiments. The first set of experiments comprises time-of-flight spectrum measurements of spheres pulsed by 14-MeV neutrons performed by Lawrence Livermore National Laboratory in the early 1970s. The second set of experiments comprises spontaneous fission neutron attenuation measurements in relatively simple geometries with varying shield thicknesses performed by Ueki et al. in the early 1990s. First, traditional constructive solid geometry (CSG) models are analyzed to ensure agreement with experimental values and to form a basis of comparison with UM results. For the pulsed sphere experiments, a series of UM calculations is performed using first-order tetrahedral elements with various levels of mesh refinement. For the Ueki experiments, purely CSG, purely UM, and hybrid CSG/UM calculations are performed using first- and second-order tetrahedral and hexahedral elements. In the purely UM cases, two different meshing algorithms are used to specify the first-order tetrahedral mesh. The pulsed sphere calculated and experimental time-of-flight spectra agree with p-values >0.999 when compared using χ^2 goodness-of-fit tests. Furthermore, the UM results show discrepancies with the experimental values comparable to the CSG cases. The Ueki neutron attenuation calculated values using track-length and point detector tallies agree with the experimental values within 1σ with a single exception that agrees well within 2σ. As such, we conclude that the results for the CSG and UM calculations agree among themselves and with the experimental quantities when considering the associated statistical uncertainties.*

Keywords — *Experimental benchmark comparison, MCNP, unstructured mesh.*

Note — *Some figures may be in color only in the electronic version.*

I. INTRODUCTION

This paper reports results for calculations performed using MCNP6's unstructured mesh (UM) capabilities based on two sets of experimental benchmarks. This work is used to broaden the verification and validation (V&V) suite of problems for MCNP6's UM capabilities and, along the way, help to improve the robustness of the UM tracking algorithms by showing weaknesses in the point detector routines that have subsequently been rectified. A subset of the cases herein is expected to be included in a future MCNP6 V&V suite release.

The first set of experiments was performed at Lawrence Livermore National Laboratory (LLNL) in the early 1970s and consists of time-of-flight spectrum measurements resulting from spheres of various materials pulsed with 14-MeV neutrons.[1] These experiments are chosen because they provide validation of time-dependent quantities (something not yet

*E-mail: jkulesza@umich.edu

extensively tested with MCNP6's UM capabilities). Also, these experiments use geometries that are traditionally difficult to model with UM (i.e., curved surfaces and/or thin spherical shells). These features allow us to examine the sensitivity of the results to various levels of mesh refinement relative to the traditional constructive solid geometry (CSG) results in the current shielding validation suite.

The second set of experiments discussed herein consists of spontaneous fission neutron attenuation sensitivity measurements performed by Ueki et al. in the early 1990s (Ref. 2). Note that this set of experiments is subtly different from the benchmark experiments described in Ref. 3 (noted to avoid confusion because of the similarity and the greater availability of Ref. 3). Regardless, the experimental benchmark used herein is chosen because it is characterized by simple but nontrivial geometry and continues to be used to validate both transport methods[4] and nuclear data[5] and is thus well studied and understood.

Both sets of experiments are analyzed using CSG and UM geometry. For the pulsed spheres, the UM consists of strictly first-order tetrahedral elements with various levels of mesh refinement. However, for the Ueki benchmark the UM consists of first- and second-order (linear and quadratic) tetrahedral and hexahedral elements and a single level of refinement for each element type. As such, this paper provides a set of results for two experimental benchmarks that can be used to validate time-dependent and time-independent neutron behavior for a variety of UM element types.

II. LLNL PULSED SPHERE DESCRIPTIONS

The LLNL pulsed sphere experiments studied a series of materials in various configurations. Sometimes identical materials in different geometric configurations were used to investigate pulse spectrum behavior resulting from attenuation through various thicknesses of the material. Of the experiments conducted, six unique material and geometric configurations are selected for analysis herein. The experiments analyzed will be described specifically in Secs. II.B through II.G with the MCNP6 validation suite identifiers in parentheses should the reader wish to locate the CSG models within his or her existing MCNP6/Testing/VALIDATION_SHIELDING directory.

II.A. Experimental Setup Overview

All spheres feature a channel through half of the sphere that permits insertion of the target assembly used to produce the 14-MeV source neutrons. Assuming that the target assembly enters the sphere through the channel from the $+x$ direction, the detector package is positioned relative to the $-x$ direction. Note that the detector package is modeled as a ring detector within MCNP6 because of geometric and source symmetry. For each experiment, the detector is either a Pilot-B or a NE213 scintillator and associated hardware, with the response functions given in Ref. 6. When describing the spherical geometry, the dimensions are given in terms of 14-MeV neutron mean free paths (mfp) along the flight path from the source to the detector and also the outer radius of the sphere in centimeters.

II.B. Beryllium Sphere (BE08/lps_berl)

The beryllium sphere with a thickness of 0.8 mfp (outer radius of 12.58 cm) consists of a spherical shell with a cylindrical channel and spherical hollow core as shown in Fig. 1a. A Pilot-B detector with a 1.6-MeV cutoff energy and full-width at half-maximum (FWHM) resolution of 4 ns is positioned 30 deg off-axis with a flight path distance of 765.2 cm. The detector captured results from 137 to 409 ns (corresponding to neutron energies of 1.8 to 16.7 MeV).

II.C. Carbon Sphere (C29/lps_carbon)

The carbon sphere with a thickness of 2.9 mfp (outer radius of 20.96 cm) consists of a spherical shell with a cylindrical and tapered round channel leading to the center as shown in Fig. 1b. A NE213 detector with a 1.6-MeV cutoff energy and FWHM resolution of 4 ns is positioned 30 deg off-axis with a flight path distance of 766.0 cm. The detector captured results from 141 to 409 ns (corresponding to neutron energies of 1.8 to 15.8 MeV).

II.D. Concrete Sphere (CCR20/lps_conc)

The concrete sphere with a thickness of 2.0 mfp (outer radius of 21 cm) consists of a spherical shell with a tapered round channel leading to a hollow spherical center cavity as shown in Fig. 1c. A NE213 detector with a 1.6-MeV cutoff energy and FWHM resolution of 3 ns is positioned 120 deg off-axis with a flight path distance of 975.4 cm. The detector captured results from 185 to 491 ns (corresponding to neutron energies of 2.1 to 14.9 MeV).

II.E. Iron Sphere (FE09/lps_iron)

The iron sphere with a thickness of 0.9 mfp (outer radius of 4.46 cm) consists of a spherical shell with a tapered round channel leading to the center as shown in Fig. 1d. A NE213 detector with a 1.6-MeV cutoff energy and FWHM resolution of 3 ns is positioned 30 deg off-axis with a flight path distance of 766.0 cm. The detector

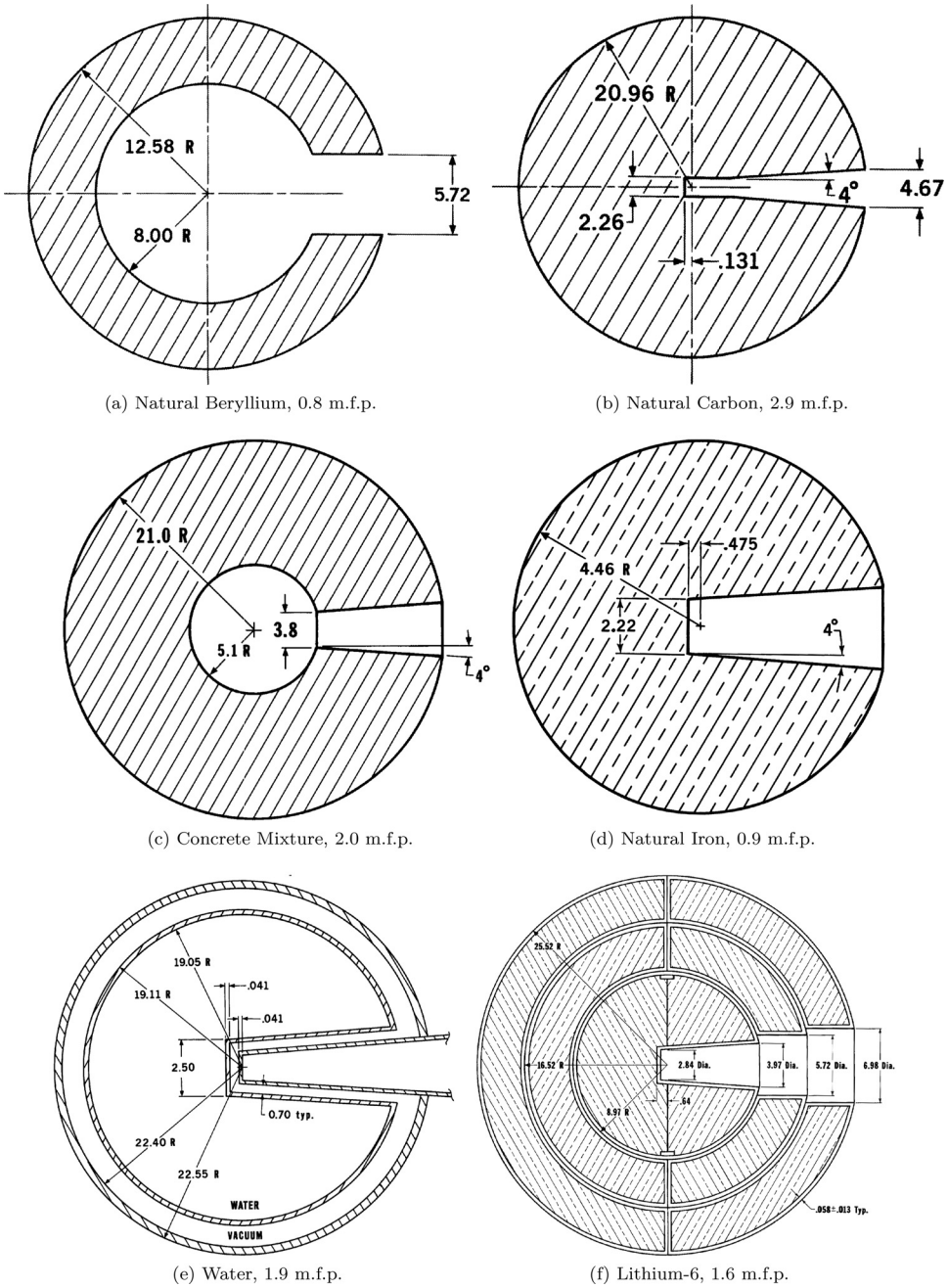

(a) Natural Beryllium, 0.8 m.f.p.

(b) Natural Carbon, 2.9 m.f.p.

(c) Concrete Mixture, 2.0 m.f.p.

(d) Natural Iron, 0.9 m.f.p.

(e) Water, 1.9 m.f.p.

(f) Lithium-6, 1.6 m.f.p.

Fig. 1. Pulsed sphere geometries reformatted from Ref. 1 (dimensions are in units of centimeters).

captured results from 137 to 417 ns (corresponding to neutron energies of 1.8 to 16.8 MeV).

II.F. Water Sphere (H2O19/lps_water)

The water sphere with a thickness of 1.9 mfp (outer radius of 22.55 cm) consists of a spherical steel shell (0.15 cm) filled with water surrounded by another steel shell (0.06 cm) with a vacuum between both shells. Each shell has a tapered round channel leading to the center as shown in Fig. 1e. A Pilot-B detector with a 1.6-MeV cutoff energy and FWHM resolution of 5 ns is positioned 30 deg off-axis with a flight path distance of 754.0 cm. The detector captured results from 126 to 392 ns (corresponding to neutron energies of 1.9 to 19.3 MeV).

II.G. Lithium Sphere (LI616/lps_lith)

The ^{6}Li sphere with a thickness of 1.6 mfp (outer radius of 25.52 cm) consists of three steel shells (each

0.058 cm thick) with lithium filling the region between each shell. The inner shell has a tapered round channel leading to the center with the two outer shells having a cylindrical channel as shown in Fig. 1f. A Pilot-B detector with a 1.6-MeV cutoff energy and FWHM resolution of 4 ns is positioned 30 deg off-axis with a flight path distance of 765.2 cm. The detector captured results from 133 to 409 ns (corresponding to neutron energies of 1.8 to 17.8 MeV).

II.H. CSG and UM Model Overview

The aforementioned six pulsed sphere experiments were also analyzed previously using two different levels of geometric, material, source, and tally specificity as part of the MCNP6 shielding validation suite.[7] The models with less specificity (i.e., "Legacy") models contain only the geometry of the spheres themselves whereas the "Detailed" models contain the sphere, the target assembly that emits the 14-MeV neutrons, and some external geometry such as beamlines. The Detailed models also contain detailed source and tally specifications relative to the Legacy models and somewhat different material compositions.

For the UM models analyzed herein, only the spherical geometry is modeled, so the Legacy models form the fairest basis for comparison. However, UM results are compared to the CSG Legacy models (which had time-of-flight tallies added), the CSG Detailed models (which have preexisting explicit time-of-flight tallies), and newly constructed CSG hybrid models that contain only the simplistic geometry but the source, material, and tally definitions from the Detailed models. All UM solid models are constructed using SpaceClaim Engineer 2014 (Ref. 8), which are then meshed and used to generate MCNP6 input files with Attila4MC (Ref. 9). When generating the UM, Attila4MC's Curvature Refinement (advanced) option is used extensively to specify maximum d/h (i.e., the distance d of the model edge curve from the mesh edge divided by the mesh size h) and minimum mesh edge length. For each experiment, various refinement levels are used to determine the sensitivity of results to the mesh size. The refinement levels, generating parameters, and resulting mesh descriptions are summarized in Table I. Like the preexisting validation suite cases, no variance reduction is introduced beyond the default techniques enabled (i.e., weight cutoff and implicit capture for the random transport and the default point detector roulette game) for both CSG and UM calculations. Materials and sources in the UM cases are defined consistent with the Legacy CSG models.

Note that for processing the MCNP6-calculated results, a multistep process is used to properly normalize the time spectra. Following a procedure described by work performed in 2011 (Ref. 10), time-of-flight spectra

TABLE I

Pulsed Sphere UM Parameter Summary*

Experiment	Refinement	Maximum d/h	Nodes	Elements
Beryllium	Fine	0.005	15517	70151
	Medium	0.010	8759	36249
	Coarse	0.020	3260	15074
Carbon	Fine	0.005	10297	46190
	Medium	0.010	6583	27923
	Coarse	0.020	4469	18754
Concrete	Fine	0.005	16112	73409
	Medium	0.010	7846	33695
	Coarse	0.020	4684	19585
Iron	Very Fine	0.0025	9332	42742
	Fine	0.005	3117	12470
	Medium	0.010	720	2777
	Coarse	0.020	217	885
Water	Fine	0.005	48018	195071
	Medium	0.010	41552	167939
	Coarse	0.020	25790	99104
Lithium	Fine	0.005	110790	376903
	Medium	0.010	77460	274125
	Coarse	0.020	34411	123293

*Minimum edge length = 0.010 cm.

are renormalized with the fm card using the following procedure that necessitates three sequential calculations:

1. Set all cell materials and densities corresponding to air. Calculate the normed average tally per history $\bar{x}_{Air}$ reported by MCNP6 for the time-of-flight spectrum tally.

2. Run the nominal material calculation with an fm card equivalent to $1/\bar{x}_{Air}$, and integrate the resulting discrete time-of-flight spectrum, which is denoted $S_{Calc.}$.

3. Run the nominal material calculation with an fm card equivalent to $\frac{1}{\bar{x}_{Air}} \frac{S_{Exp.}}{S_{Calc.}}$, where $S_{Exp.}$ is the integral of the discrete experimental spectrum.

For the purposes herein, all normalization values are considered to be "best estimate," so no error propagation to the final results is performed. When performing normalizations and comparisons, it is important to recognize that the benchmark times are given in nanoseconds whereas MCNP6 specifies times in "shakes" where 1 shake is equivalent to 10 ns. Nevertheless, in all cases the calculated tally time bin structure is consistent with the corresponding experimental time bin structure.

III. UEKI BENCHMARK DESCRIPTION

The Ueki benchmark suite is a series of experiments characterized by a small spontaneous fission ^{252}Cf source

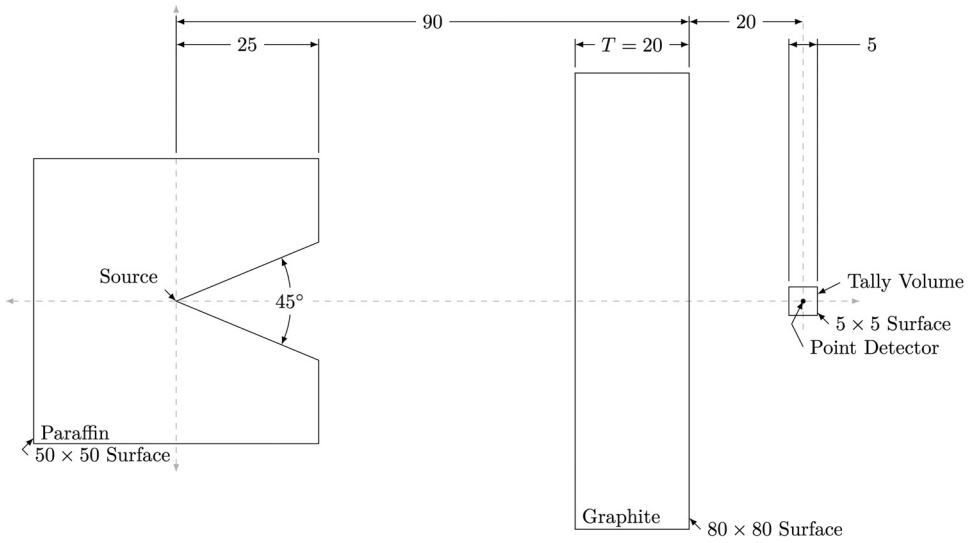

Fig. 2. Ueki benchmark geometry (dimensions are in units of centimeters).

centered within a paraffin cube with a conical cutout facing a detector, with one or several shields of thickness T between the source and detector as shown in Fig. 2. Of the configurations provided in the experimental description,[2] this analysis focuses on those configurations with a single graphite shield of either thickness $T = 2$, 5, 10, 15, 20, 25, 30, or 35 cm. This benchmark was most recently analyzed in Ref. 4 where it is noted that tabulated results are not provided for the cases with the graphite shield. As such, the lin-log plot provided in Ref. 4's Fig. 7-2 is digitized to extract the experimental dose attenuation factors for graphite. When this digitization is performed, a conservative 5% uncertainty is assigned to account for experimental and digitization errors.

The experiments are modeled using both CSG and UM with a small cubic F4 (track-length) tally with an F5 (point detector) tally centered within the cube; Ref. 4 did likewise but for CSG only. Unlike Ref. 4, no variance reduction is performed beyond the default techniques enabled (i.e., weight cutoff and implicit capture for the random transport and the default point detector roulette game). This approach is taken in order to understand the unperturbed rate of problem convergence for both geometries. Both the CSG and the UM models use materials for paraffin, graphite, and air based on the compositions and densities provided in Ref. 11. For both geometries, the source is positioned at $x = 0.001$ cm in order to prevent it from being coincident with CSG cell or UM pseudocell boundaries. The source is specified with an energy distribution following the MCNP6 Watt fission spectrum (function -3) using MCNP6 distribution parameters $a = 1.025$ and $b = 2.926$. When specifying the two tallies, the dose response function from Ref. 12 is used, and the results are normalized to Sv · h^{-1} · source-particle^{-1}. Because the benchmark results are given as dose attenuation factors, once the calculations are performed, the calculated shielded results are normalized to the unshielded value. Finally, the calculated values are normalized relative to the experimental values for easier interpretation.

Two methods for generating the UM input file are used here. At present, MCNP6 only supports UM specified using an Abaqus mesh input file format.[13] As such, the analyst can use Abaqus to create the mesh input file after creating (or importing) the geometry, assigning materials and element sets, and creating the mesh. More details regarding working with MCNP6's UM capabilities in this regard are given in Ref. 14 with a direct illustration using Abaqus (to create geometry similar to the Ueki experiment with a 20-cm graphite shield) given in Ref. 15. Once the Abaqus mesh input file is created, the um_pre_op utility provided with MCNP6 can be used to generate a skeleton MCNP6 input file. Alternatively, one can use Attila4MC to prepare Abaqus-formatted UM and MCNP6 input files as done with the pulsed sphere experiments. Note that Abaqus is capable of generating mesh using first- and second-order tetrahedral, pentahedral, and hexahedral elements whereas Attila4MC is only capable of generating mesh using first-order tetrahedrons.

Abaqus is used to generate UM using first- and second-order tetrahedral and hexahedral elements to compare the effect (which should be minimal) of using different element types. Furthermore, hybrid geometry cases are created with either the paraffin or shield/detector defined as CSG and the remainder as UM to validate cases where it is appropriate to combine CSG and UM. Regardless, when generating a mesh with Abaqus, a "seed" is needed to roughly define edge length. When tetrahedral and hexahedral mesh (both first- and second-order) are

seeded, the same seed value is used, so the resulting mesh is on as consistent a basis as possible. Some minor differences are expected in the results because the conical cutout in the paraffin cannot be represented exactly using UM and particle positions on the surfaces will be different and subsequently affect the particle tracking.

In addition, Attila4MC is used to generate UM using first-order tetrahedral elements in order to see the effect of a different meshing algorithm on the results. Like the pulsed sphere experiments, when using Attila4MC, Curvature Refinement is applied with a maximum $d/h = 0.02$ and a minimum edge length of 1 cm. The Attila4MC-generated models are entirely of the UM variety since Attila4MC does not handle CSG; ample validation of hybrid geometries is provided with the Abaqus model calculations.

IV. CALCULATION RESULTS

Each of the calculations uses a consistent "bleeding edge" (i.e., nightly build) version of MCNP6, version 6.1.2. The latest nuclear data libraries supplied with MCNP6 are used. The pulsed sphere calculations use libraries consistent with the validation suite cases (ACTIA and ENDF66A based on ENDF/B-VI.8 and ENDF/B-VI.0, respectively). The Ueki calculations use the default library for each material's constituent isotope (ENDF71X, ENDF7SAB, and RMCCSA based on ENDF/B-VII.1, ENDF/B-VII.0, and LLNL evaluations, respectively). All calculations are performed on the Los Alamos National Laboratory Mapache supercomputer. Mapache consists of 592 compute nodes hosting dual-socket quad-core Intel Nahalem processors (4736 processing cores total) interconnected with InfiniBand with calculations distributed through the Moab Workload Manager. Each pulsed sphere CSG and UM calculation used 8 processors, and each Ueki calculation used between 16 and 64 processors in order to balance queue throughput and speed of execution while keeping all calculations well below an administratively imposed wall time limit. The pulsed sphere Legacy CSG models use 1 million histories with Hybrid, and Detailed CSG models use 10 million (all consistent with the MCNP6 validation suite). All pulsed sphere and Ueki UM models use 1 million histories.

IV.A. Pulsed Sphere Results

The pulsed sphere calculated spectra are shown in Fig. 3 for the six experiments studied. Note that the line plots are colored based on the ColorBrewer2 8-class Paired color set[16] in the electronic version of this paper. Additional effort is not made to differentiate the data sets (in the print or electronic versions of this paper) on a given plot because of the generally high level of agreement for the purposes of our comparisons herein.

For all calculations, the agreement between the experimental and the calculated spectra is qualitatively confirmed through visual inspection. One abnormality is apparent in Fig. 3c around 310 ns—a step change in the calculated response relative to the benchmark. This artifact is not visible in recent published work (Fig. 48 of Ref. 17), and it would be interesting to identify the reason for this. Regardless, using a χ^2 goodness-of-fit test shows that unnormalized and normalized calculated and experimental spectra agree with p-values >0.999 in all cases, which supports a null hypothesis that a given calculated spectrum behaves comparably to the experimental spectrum.

Next, the fractional errors ϵ between the calculated and the experimental spectra are determined with

$$\epsilon = \frac{\int_0^\infty [f_{Exp.}(t) - f_{Calc.}(t)]^2 dt}{\int_0^\infty [f_{Exp.}(t)]^2 dt} \rightarrow \frac{\sum_t (f_{t,Exp.} - f_{t,Calc.})^2}{\sum_t (f_{t,Exp.})^2} \quad (1)$$

by recognizing that all time bin widths are identical and that there are an equal amount of bins in the calculated and the experimental results. These fractional errors are shown in Table II, and it should be recognized that unlike previous work in Ref. 10, no points are excluded from either the χ^2 p-value or the fractional error calculations. Furthermore, the error observed in the UM models agrees most closely with the Legacy models while the Detailed and Hybrid models behave similarly. Because the geometry in the Legacy and Hybrid models is identical, differences between the UM calculations and the more detailed CSG and experimental results can be attributed to material, source, and external geometry differences rather than

TABLE II

Fractional Errors for Pulsed Sphere Calculated Spectra

	CSG			UM		
Experiment	Detailed	Hybrid	Legacy	Fine	Medium	Coarse
Beryllium	0.136	0.137	0.054	0.054	0.054	0.054
Carbon	0.161	0.165	0.092	0.093	0.092	0.092
Concrete	0.146	0.156	0.244	0.243	0.243	0.241
Iron[a]	0.079	0.093	0.210	0.248	0.248	0.249
Water	0.234	0.234	0.175	0.192	0.191	0.191
Lithium	0.013	0.013	0.011	0.009	0.009	0.009

[a]Very fine UM fractional error: 0.248.

the spherical geometry. Regardless, we can conclude that the pulsed sphere UM models adequately agree with the CSG and experimental results. This statement is true for all levels of mesh refinement, suggesting a relatively low sensitivity to mesh refinement as long as the mesh is a reasonable representation of the intended configuration and does not feature any defects or artifacts. For this work, the UM was generated finely enough to keep the mass of the spheres consistent with the CSG geometry within 1% for the spheres, within 2% for the water sphere's shell, and within 3% for the lithium sphere's shell.

IV.B. Ueki Neutron Attenuation Results

As noted previously, the Ueki calculations can be roughly divided into three groups: those with strictly

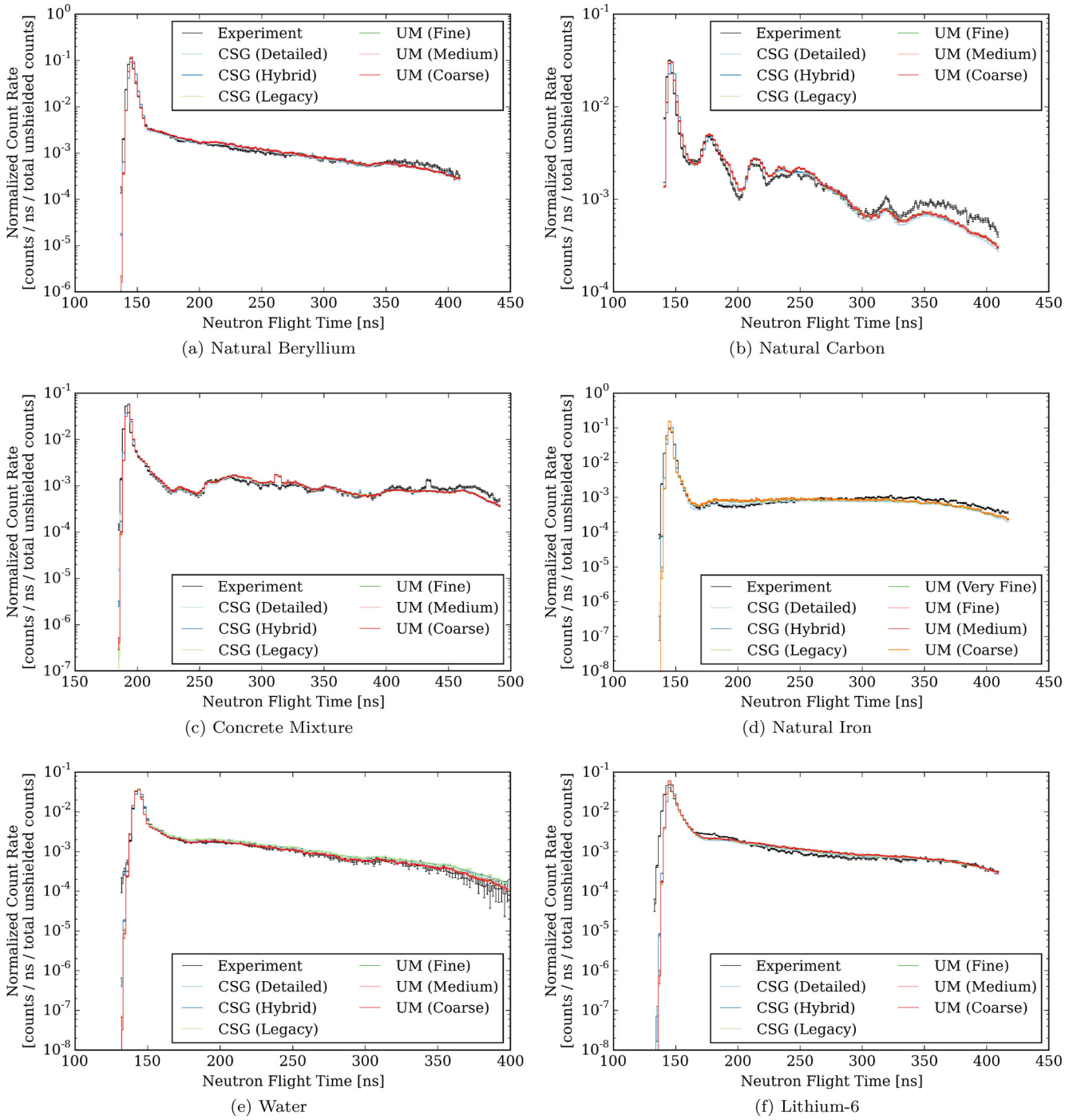

(a) Natural Beryllium

(b) Natural Carbon

(c) Concrete Mixture

(d) Natural Iron

(e) Water

(f) Lithium-6

Fig. 3. Pulsed sphere time-of-flight spectra for CSG and UM cases (all results include $\pm 1\sigma$ uncertainty bars).

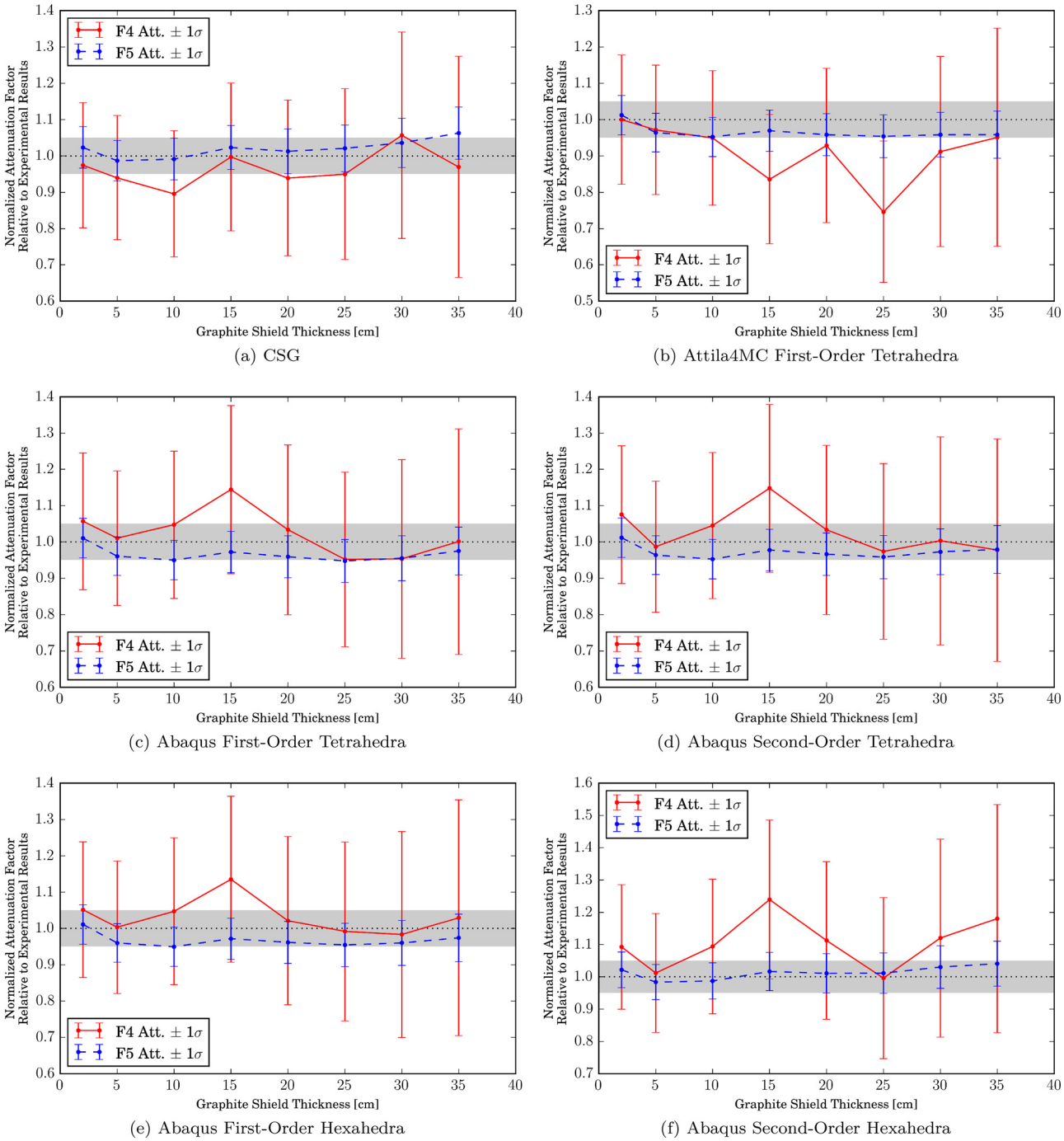

Fig. 4. Normalized Ueki neutron attenuation curves for CSG and purely UM calculations relative to experimental values.

UM, those with the paraffin as UM and the shield/detector as CSG, and those with the paraffin as CSG and the shield/detector as UM. The results for the strictly UM (and strictly CSG) calculations are shown in Fig. 4. The results for the hybrid cases with the paraffin as UM are shown in Fig. 5, and the results for the hybrid cases with the paraffin as CSG are shown in Fig. 6.

In Fig. 4, both the F4 and F5 tallies show agreement with the experimental attenuation values within 1σ with the sole exception of the Attila4MC F4 tally corresponding to a 25-cm-thick graphite shield (which narrowly misses the 1σ criterion but agrees well within 2σ). For the hybrid case results shown in Figs. 5 and 6, the F4 and F5 tallies show agreement with the experimental attenuation values within 1σ without exception. Observe that

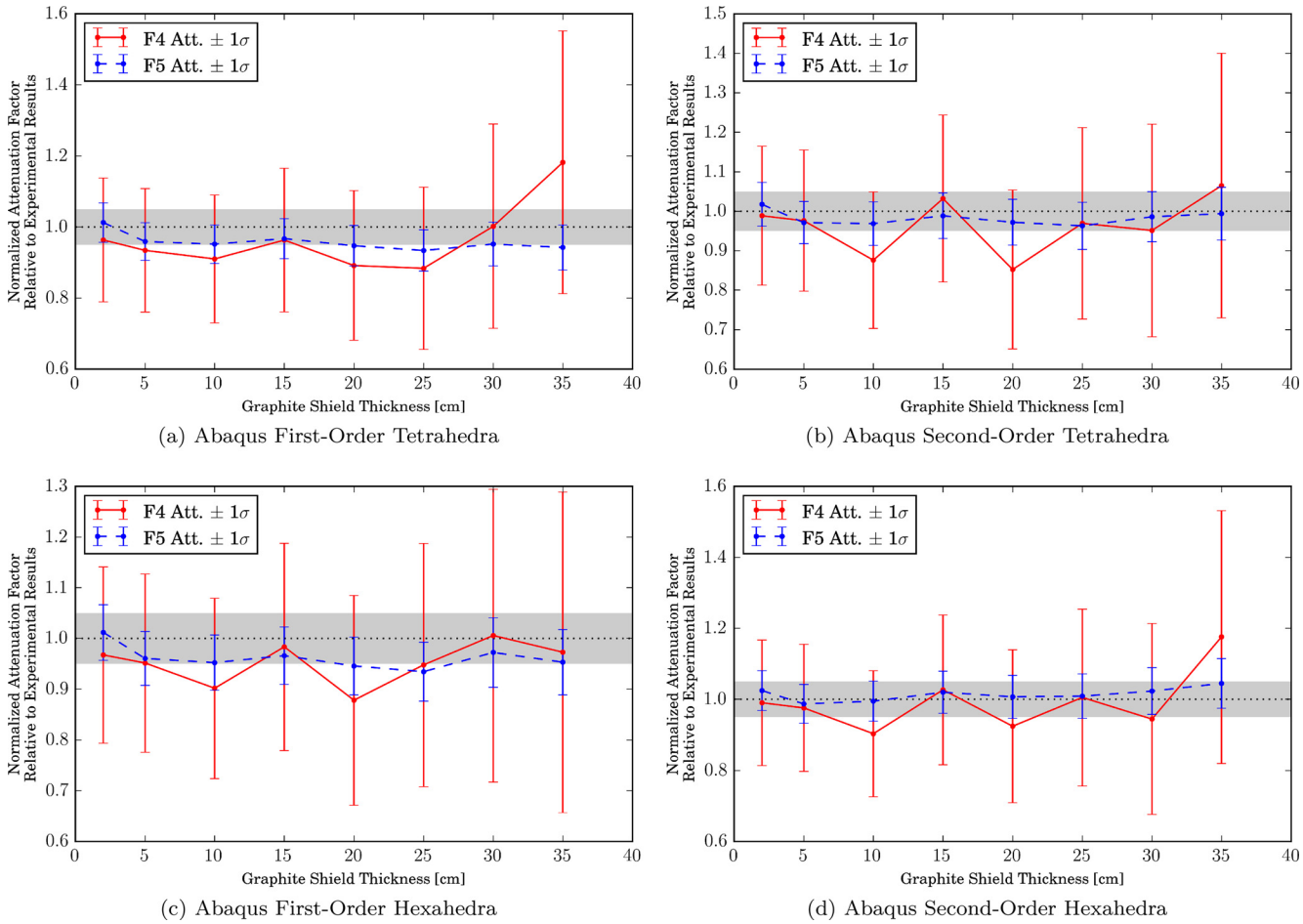

(a) Abaqus First-Order Tetrahedra

(b) Abaqus Second-Order Tetrahedra

(c) Abaqus First-Order Hexahedra

(d) Abaqus Second-Order Hexahedra

Fig. 5. Normalized Ueki neutron attenuation curves for hybrid CSG/UM calculations (paraffin as UM and shield/detector as CSG) relative to experimental values.

the results shown in Fig. 5 are identical because the UM represents purely Cartesian components, and because of the identical seeding, the mesh elements have the same boundaries. As such, particles that make it to either tally will undergo identical surface crossings and thus register the same score.

In addition, perspective half-space qualitative F4 flux edits are provided in Fig. 7 for the purely UM cases with first-order elements to (a) provide an overall view of the flux behavior to validate its appropriateness and (b) illustrate one of the benefits of using UM: minimal-overhead geometry-specific UM-based results visualization. Only linear elements are shown for demonstration purposes, but other UM results appear similarly. Looking at the mesh and edits, a couple of observations can be made:

1. The Abaqus-generated mesh features the graphite shield divided into a series of shields (parts) in order to reuse identical mesh input files in a number of cases. Each of the parts is assigned a different material (graphite or air) within MCNP6 to represent the various shield thicknesses. While this leads to an unnecessarily refined mesh within the shield, it reduces the file handling (and subsequent quality control) burden.

2. The Curvature Refinement feature within Attila4MC has a clear local effect on the mesh when comparing the mesh size around the conical cutout in the paraffin versus those in the shield. This feature provides a convenient way to allow precise geometric representation without unduly fine mesh throughout the model.

3. Because of how the F4 flux edits are calculated, a coarse mesh (such as the one shown in the Attila4MC shield) will yield less information than a fine mesh (such as in the Abaqus cases). The coarse mesh is adequate to represent the geometry; however, it is less useful when visualizing the resulting particle distribution.

As such, the user is cautioned to specify the UM resolution considering both appropriate representation of the geometry versus mesh size (and thus element count)

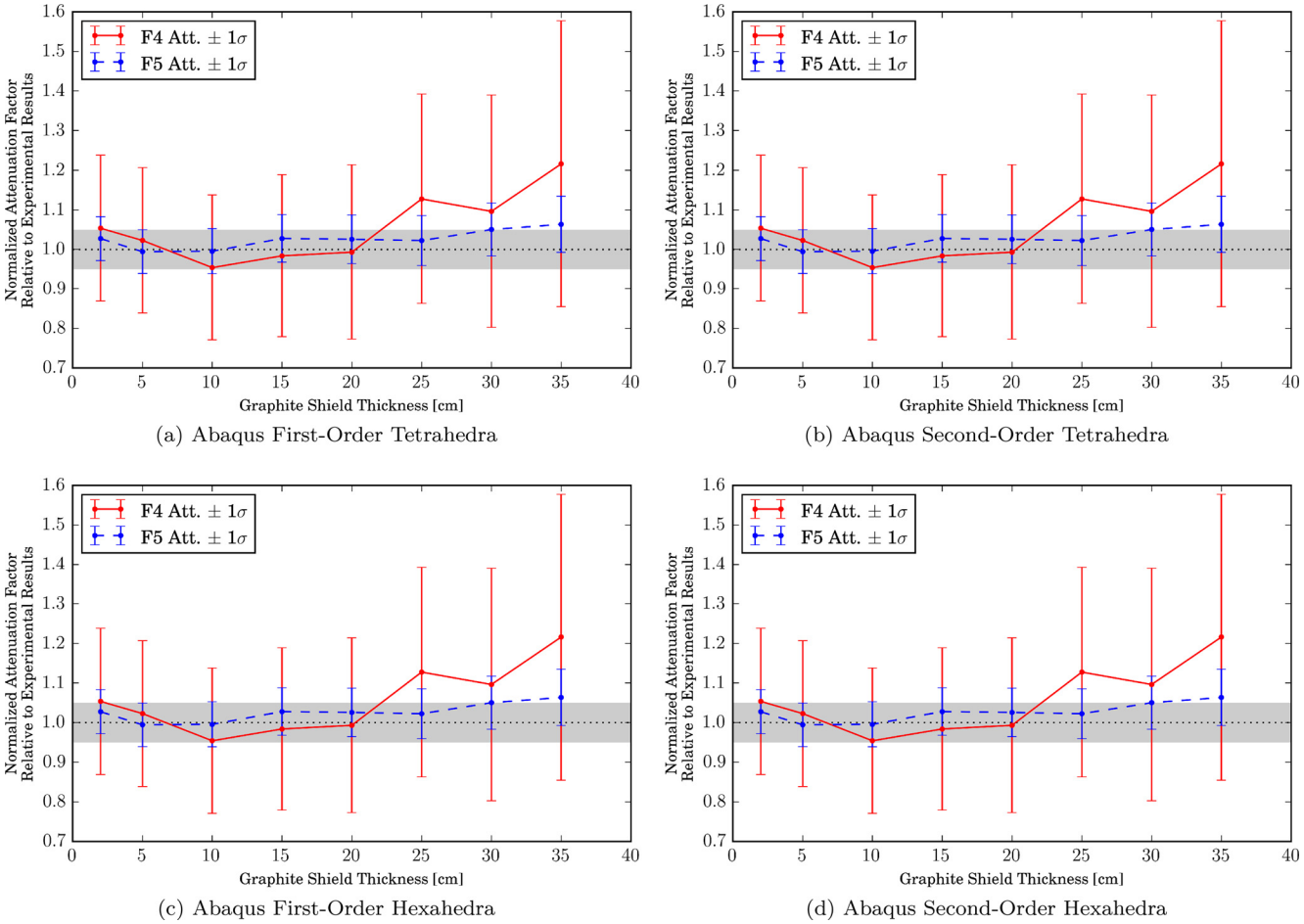

(a) Abaqus First-Order Tetrahedra

(b) Abaqus Second-Order Tetrahedra

(c) Abaqus First-Order Hexahedra

(d) Abaqus Second-Order Hexahedra

Fig. 6. Normalized Ueki neutron attenuation curves for hybrid CSG/UM calculations (paraffin as CSG and shield/detector as UM) relative to experimental values.

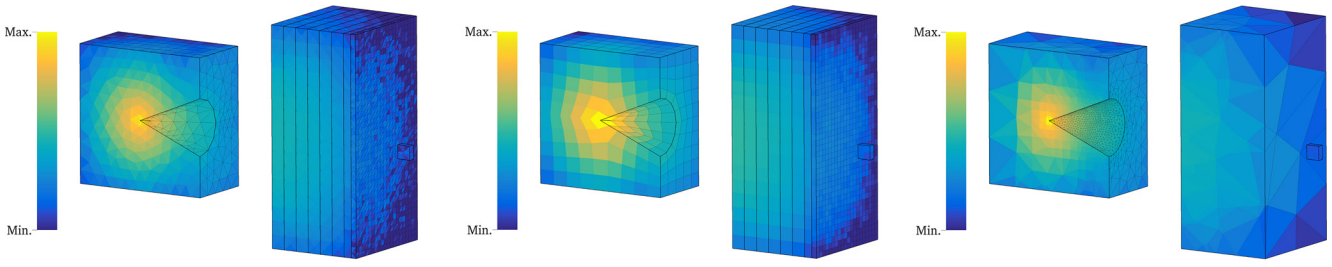

(a) Abaqus First-Order Tetrahedra

(b) Abaqus First-Order Hexahedra

(c) Attila4MC First-Order Tetrahedra

Fig. 7. Ueki perspective half-space neutron flux (F4) element-wise edits.

and the intended use of the UM edits from a postprocessing and visualization standpoint.

V. CONCLUSIONS

The pulsed sphere calculated and experimental time-of-flight spectra agree with a p-value >0.999 when compared with χ^2 goodness-of-fit tests with the UM cases showing discrepancies from the experiment comparable to the discrepancies shown by the CSG cases. The Ueki neutron attenuation calculated values using F4 and F5 tallies agree with the experimental values within 1σ except for a single point that agrees well within 2σ. Qualitatively, we can see that the behavior of all calculated results in terms of magnitude and trends is reasonable. As such, we conclude that the results for the CSG and UM calculations agree among themselves and with

the experimental quantities when considering the associated statistical uncertainties. This conclusion and work thus extend the V&V basis for MCNP6's UM capabilities.

Future work includes performing equivalent analyses with first- and second-order pentahedral elements. This is not done in the present work because these elements tend to be used much less frequently than tetrahedral and hexahedral elements, and the tracking routines for them are a combination of the tetrahedral and hexahedral routines. It would also be interesting to investigate the cause for the step in the concrete sphere time-of-flight spectrum at ~310 ns. While it is likely not the result of a nuclear data issue, it would also be interesting to investigate the effect of using the most current nuclear data on the time-of-flight spectra for all spheres investigated herein similar to what was done in Ref. 17. Finally, no variance reduction is performed for the analyses herein. While it is unnecessary for the pulsed spheres, it would be compelling to investigate the behavior and figure-of-merit of the tallies when different variance-reduction techniques are applied to the Ueki benchmark. These techniques might include (pseudo)cell-based importances or weight windows and mesh-based weight windows generated with the MCNP6 weight window generator or an external utility such as Attila4MC and/or ADVANTG. Note that one advantage (no pun intended) to mesh-based weight windows is that they transcend the geometry type used, so a single set of weight windows can be applied to CSG, UM, or hybrid geometry calculations.

Acknowledgments

The authors wish to thank J. M. Risner of Oak Ridge National Laboratory for providing electronic reference cases for the Ueki experiments in order to validate preexisting input parameters and to confirm the experimental configuration. The authors also thank G. A. Failla and I. M. Davis of Varian Medical Systems for providing the licenses and expert insights that permitted the use of SpaceClaim and Attila4MC for this work.

References

1. C. WONG et al., "Livermore Pulsed Sphere Program: Program Summary Through July 1971," UCRL-51144, Rev. 1, Lawrence Livermore National Laboratory (1972).
2. K. UEKI, A. OHASHI, and Y. ANAYAMA, "Neutron Shielding Ability of KRAFTON N2–Mannan—KRAFTON N2 Sandwich-Type Material and Others," *Proc. Radiation Protection and Shielding Division Topl. Mtg.*, Pasco, Washington, April 26–May 1, 1992, p. 130, American Nuclear Society (1992).
3. K. UEKI et al., "Systematic Evaluation of Neutron Shielding Effects for Materials," *Nucl. Sci. Eng.*, **124**, 455 (1996); http://dx.doi.org/10.13182/NSE124-455.
4. S. W. MOSHER et al., "ADVANTG—An Automated Variance Reduction Parameter Generator," ORNL/TM-2013/416, Oak Ridge National Laboratory (2013).
5. J. M. RISNER et al., "Production and Testing of the VITAMIN-B7 Fine-Group and BUGLE-B7 Broad-Group Coupled Neutron/Gamma Cross-Section Libraries Derived from ENDF/B-VII.0 Nuclear Data," NUREG/CR-7045, ORNL/TM-2011/12, Oak Ridge National Laboratory (2011).
6. E. F. PLECHATY and R. J. HOWERTON, "Calculational Models for LLL Pulsed Spheres (CSEWG Shielding Benchmark Collection No. SDT 10)," UCID-16372, Lawrence Livermore National Laboratory (1973).
7. J. T. GOORLEY et al., "Initial MCNP6 Release Overview—MCNP6 Version 1.0," LA-UR-13-22934, Los Alamos National Laboratory (2013).
8. "SpaceClaim Engineer 2014," SpaceClaim Corporation (2014); http://www.spaceclaim.com/en/default.aspx (current as of Sep. 11, 2015).
9. "Attila with MCNP Integration: Attila4MC," Varian Medical Systems (2015); http://www.transpireinc.com/html/attila (current as of Sep. 11, 2015).
10. A. S. BENNETT and B. C. KIEDROWSKI, "Revisiting the MCNP Shielding Validation Suite," LA-UR-11-04540, Los Alamos National Laboratory (2011).
11. R. J. McCONN, JR., et al., "Compendium of Material Composition Data for Radiation Transport Modeling," PNNL-15870, Rev. 1, Pacific Northwest National Laboratory (2011).
12. ANSI/ANS 6.1.1-1977, "Neutron and Gamma-Ray Flux-to-Dose-Rate Factors," American Nuclear Society, La Grange Park, Illinois (1977).
13. "Abaqus/CAE 6.12 Online Documentation," Dassault Systèmes Simulia Corporation (2012).
14. R. L. MARTZ, "The MCNP6 Book on Unstructured Mesh Geometry: User's Guide," LA-UR-11-05668, Rev. 8, Los Alamos National Laboratory (2014).
15. J. A. KULESZA and R. L. MARTZ, "MCNP6 Unstructured Mesh Tutorial Using Abaqus/CAE 6.12-1," LA-UR-15-25143, Los Alamos National Laboratory (2015).
16. C. A. BREWER, "Color Brewer 2"; http://www.colorbrewer2.org/ (accessed Aug. 10, 2015).
17. R. D. MOSTELLER, S. C. FRANKLE, and P. G. YOUNG, "Data Testing of ENDF/B-VI with MCNP: Critical Experiments, Thermal-Reactor Lattices, and Time-of-Flight Measurements," LA-UR-96-2143, Los Alamos National Laboratory (1996).